Memorias del Congreso Nacional de Control Automático
ISSN: 2594-2492

An improved passivity-based control for inverter-based Microgrids ⋆

Isaac Ortega-Velázquez, * **Sofía Avila-Becerril,** *
Gerardo Espinosa-Pérez, * **Rodrigo Ojeda** *

* *Universidad Nacional Autónoma de México, Facultad de Ingeniería-UNAM 04510 Ciudad de México, México*

Abstract: In this paper, we focus on the primary control of inverter-based microgrids. The controller consists of the interconnection of two passivity-based controllers, one that adds a virtual impedance and another that achieves voltage regulation. The equal power-sharing is reached with the addition of a droop-type controller. Numerical evaluations show the performance of the proposed control algorithm.

Keywords: AC Microgrids, Passivity-based, Hamiltonian, Output Impedance.

1. INTRODUCTION

A Microgrid (MG) is a small-scale grid formed of distributed generation units (DGU), power converters, lines, electrical energy storage (EES), and loads, with the ability to self-supply, island, distribute, and regulate the flow of electricity to the loads (Rojas and Rousan [2017], Han et al. [2016]). In terms of control, hierarchical control layers are used to obtain the desired operational requirements at different levels. This paper focuses on the primary level, which comprises an inner control loop in charge of regulating the output voltage at each inverter, and another control layer in charge of achieving equal power-sharing.

In the literature, many works related to primary control can be found (Rokrok et al. [2018], Bendib et al. [2017], De Persis and Monshizadeh [2017]). Most of these works simplify the MG's model by representing the inverters as voltage sources so that phasors describe the electrical variables (Schiffer et al. [2016]). The results are droop-type controllers designed for predominantly inductive networks. Some results include in the primary control a virtual output-impedance loop that ensures a specific behavior (inductive, capacitive, or resistive) at the line frequency (Guerrero et al. [2011], Mortezapour and Lesani [2017], Rokrok et al. [2018]).

In this paper, first, we use a modular approach to describe the MG as a port-Hamiltonian system (pH); then, we propose three steps to solve the primary control problem: an output impedance control, a tracking control, and a droop-control. Inspired by the Control by Interconnection technique (CbI), see Ortega et al. [2008], we propose to modify the output impedance by interconnecting a dynamical system (controller) through a power-preserving interconnection. A second interconnection stage is proposed to solve the tracking problem that ensures boundedness and output voltage regulation. We give a formal proof of the output impedance controller working together with the tracking controller and leave a signal available to add a droop controller. Since the designer can fix the inverters' output impedance, one can choose between a variety of droop controllers. We take the so-called robust-droop controller (Zhong [2011]) into our strategy, and we evaluate its operation in union with the other two stages.

The rest of the paper is organized as follows: Section 2 introduces the MG model from the Hamiltonian formalism. Section 3 presents the main result of the paper, the inner controller, adding the virtual impedance and the PBC for voltage and current tracking. The droop controller is presented in Section 4, and finally, some numerical simulations are given in Section 5.

2. INVERTER-BASED MICROGRID MODEL

A generic inverter located at the $k-th$ node of the MG is represented in Fig. 1.

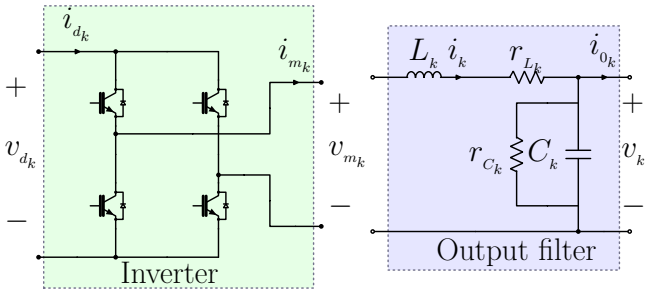

Fig. 1. General scheme of an inverter

⋆ Part of this work was supported by UNAM-PAPIIT IA105421 and UNAM-PAPIIT IN118019. Sofía Avila-Becerril (soavbec@comunidad.unam.mx)

The figure shows a single phase two-level voltage source inverter (2L-VSI) where $\mu_k \in \mathbb{R}$ is the modulation control signal. The $k-th$ inverter has as input the pair (v_{d_k}, i_{d_k}) of DC voltage and current; and it has as output the pair (v_{m_k}, i_{m_k}) of AC voltage and current. Both ports are related via the duty cycle as:

$$\begin{bmatrix} i_{dk} \\ v_{m_k} \end{bmatrix} = \begin{bmatrix} 0 & \mu_k \\ -\mu_k & 0 \end{bmatrix} \begin{bmatrix} v_{d_k} \\ i_{m_k} \end{bmatrix}. \tag{1}$$

Each 2L-VSI is connected to a second order filter with positive parameters: L_k, C_k, r_{L_k} and r_{c_k}. To obtain the model of the set of n VSI, the state variables are defined by the collection of inductor fluxes ϕ_k and the capacitor charges q_k of every VSI, such that $\phi = \text{col}\,(\phi_k)$, $q = \text{col}\,(q_k)$ and

$$x := [\phi^\top \quad q^\top]^\top \in \mathbb{R}^{2n}.$$

By recognizing that the total energy function $H : \mathbb{R}^{2n} \to \mathbb{R}^+$ of the system is

$$H(x) = \frac{1}{2} x^\top D x, \tag{2}$$

with $D = \text{bdiag}\left\{L^{-1}, C^{-1}\right\} \in \mathbb{R}^{2n\times 2n}$, $L = \text{diag}\,\{L_k\}$, and $C = \text{diag}\,\{C_k\}$, the VSI model can be written as a pH system given by:

$$\dot{x} = (J - R)\nabla H(x) + G_m v_m + G_o i_o \tag{3a}$$

$$y = G_m^\top \nabla H(x) \tag{3b}$$

with $J = \begin{bmatrix} 0 & -\mathbf{I} \\ \mathbf{I} & 0 \end{bmatrix} = -J^\top$, $G_m = \begin{bmatrix} \mathbf{I} \\ 0 \end{bmatrix}$, $G_o = \begin{bmatrix} 0 \\ -\mathbf{I} \end{bmatrix}$, $R = \text{bdiag}\left\{r_L, r_C\right\} > 0$, where $r_L = \text{diag}\{r_{L_k}\}$, $r_C = \text{diag}\{r_{c_k}^{-1}\}$, load current $i_o = \text{col}\left(i_{o_k}\right) \in \mathbb{R}^n$, $\nabla H(x)$ the vector of partial derivatives of the Hamiltonian $H(x)$ with respect to the state x, and from the vector form of (1)

$$v_m = -V_d \mu$$

where the modulation control vector $\mu = \text{col}\,(\mu_k) \in \mathbb{R}^n$, the DC input $V_d = \text{diag}\{v_{d_k}\} > 0$, and $v_m = \text{col}\left(v_{m_k}\right) \in \mathbb{R}^n$.

3. INNER CONTROLLER

Inspired by the Control by Interconnection (CbI) technique, we first present a control strategy that allows us to design the output impedance of the VSI without modifying the pH structure of the closed-loop system. The second step in the inner control strategy is to apply a tracking controller for the output voltage that also preserves the pH structure.

3.1 Control of Inverter Output Impedance

We interconnect each VSI given by the $k-th$ element of (3) to a port-Hamiltonian controller system Σ_C consisting of a virtual capacitor and two virtual resistors. The interconnection results in the virtual capacitor, with capacitance C_{v_k}, in series with the filter's inductor L_k, one resistor in series with the virtual capacitor, with resistance r_{v_k}, and another resistor in parallel with the virtual capacitor, with resistance $r_{C_{v_k}}$. If the n individual controllers are piled up, the compact form of the controller system is given by

$$\Sigma_C := \begin{cases} \dot{\zeta} = -r_{Cv}\nabla H_v(\zeta) + u_v \\ y_v = \nabla H_v(\zeta) \end{cases} \tag{4}$$

with state $\zeta \in R^n$, $u_v \in \mathbb{R}^n$, $r_{Cv} = \text{diag}\left\{r_{Cv_k}^{-1}\right\} > 0$, Hamiltonian $H_v(\zeta) : \mathbb{R}^n \to \mathbb{R}^+$

$$H_v(\zeta) = \frac{1}{2}\zeta^\top C_v \zeta, \tag{5}$$

$C_v = \text{diag}\{C_{v_k}\} > 0 \in \mathbb{R}^{n\times n}$ a controller gain, and a standard negative feedback interconnection

$$\begin{bmatrix} v_m \\ u_v \end{bmatrix} = \begin{bmatrix} -r_v & -\mathbf{I} \\ \mathbf{I} & 0 \end{bmatrix} \begin{bmatrix} y \\ y_v \end{bmatrix} + \begin{bmatrix} u \\ 0 \end{bmatrix} \tag{6}$$

where $r_v = \text{diag}\{r_{vk}\} > 0 \in \mathbb{R}^{n\times n}$ is a controller gain, and $u = \text{col}\,(u_k) \in \mathbb{R}^n$ is an external input.

Proposition 1. Consider the set of n VSI given by (3); the dynamic control law given by (4)-(6) allows to choose the output impedance of each VSI as follows:

- Inductive output impedance if $r_v = 0$, $r_{Cv} \to \infty$ and $C_v \to \infty$.
- Resisitive output impedance if $r_v \to \infty$, $r_{Cv} \to \infty$ and $C_v \to \infty$.
- Capacitive output impedance if $r_v = 0$, $r_{Cv} \to \infty$ and $C_v \to 0$.

Proof. The closed-loop system is defined in the extended state-space (x, ζ) and can be written as:

$$\dot{x}_e = (J_e - R_e)\nabla H_e(x,\zeta) + \begin{bmatrix} G_m \\ 0 \end{bmatrix} u + \begin{bmatrix} G_o \\ 0 \end{bmatrix} i_o, \tag{7a}$$

$$y_e = \begin{bmatrix} G_m^\top & 0^\top \end{bmatrix} \nabla H_e(x,\zeta) \tag{7b}$$

$x_e = \begin{bmatrix} x^\top & \zeta^\top \end{bmatrix}^\top \in \mathbb{R}^{3n}$, $R_e = \text{bdiag}\{r_L + r_v,\ r_C, r_{Cv}\} > 0$, $H_e(x,\zeta) = H(x) + H_v(\zeta)$, and $J = \begin{bmatrix} 0 & -\mathbf{I} & -\mathbf{I} \\ \mathbf{I} & 0 & 0 \\ \mathbf{I} & 0 & 0 \end{bmatrix} = -J^\top$.

Defining the currents $i_k = L_k^{-1}\phi_k$, the voltages $v_k = C_k^{-1} q_k$, and the voltage related to the virtual capacitors $v_{v_k} = C_{v_k}^{-1}\zeta_k$, with ζ_k the $k-th$ controller state, and using the steady-state of (7), the output impedance of the $k-th$ inverter is given by

$$Z_{o_k} = r_{L_k} + r_{v_k} + \frac{1}{r_{Cv_k}|Y_{Cv_k}|^2} + j\omega\left(L_k - \frac{C_{v_k}}{|Y_{Cv}|^2}\right)$$

with $Y_{C_k} = r_{C_k}^{-1} + j\omega C_k$ the admittance of the $k-th$ capacitor filter and $Y_{Cv_k} = r_{Cv_k}^{-1} + j\omega C_{v_k}$ the admittance of the $k-th$ virtual capacitor.

Since r_{L_k} is usually not significant, we can always choose the gains r_{v_k}, r_{Cv_k}, and C_{vk} to modify the output impedance Z_{o_k}.

□

3.2 Passivity-Based Tracking Controller

Following the ideas reported in Cisneros et al. [2015] and Avila-Becerril et al. [2018], we present a Passivity-Based Controller (PBC) that drives the output currents and voltages of the VSI to a desired state $x^\star$. A first step towards the development of the control strategy is the definition of the admissible trajectories that for the extended system (7) are the solutions of:

$$\dot{x}_e^\star = (J_e - R_e)\nabla H_e^\star(x_e^\star) + \begin{bmatrix} G_m \\ 0 \end{bmatrix} u^\star + \begin{bmatrix} G_o \\ 0 \end{bmatrix} i_o, \quad (8a)$$

$$y_e^\star = \begin{bmatrix} G_m^\top & 0^\top \end{bmatrix} \nabla H_e^\star(x_e^\star) \quad (8b)$$

with $u^\star \in \mathbb{R}^n$ the input that (univocally) generates the admissible behavior.

We first assume that a desired $x_e^\star \in \mathbb{R}^{3n}$ bounded and solution of (8) has been selected, Section 4 is dedicated to the design of $x_e^\star$, particularly of $x^\star \in \mathbb{R}^{2n}$. Under this condition, the control objective is to design the input $u \in \mathbb{R}^n$ in (7) such that:

$$\lim_{t\to\infty} x = x^\star \quad (9)$$

guaranteeing internal stability.

By defining the error signals as $\tilde{(\cdot)} = (\cdot) - (\cdot)^\star$, the error dynamics can be written as:

$$\dot{\tilde{x}}_e = (J_e - R_e)\nabla \tilde{H}_e(\tilde{x}_e) + \begin{bmatrix} G_m \\ 0 \end{bmatrix} \tilde{u} \quad (10a)$$

$$\tilde{y}_e = \begin{bmatrix} G_m^\top & 0^\top \end{bmatrix} \nabla \tilde{H}_e(\tilde{x}_e) \quad (10b)$$

with $\tilde{H}_e(\tilde{x}_e) = H(\tilde{x}) + H_v(\tilde{\zeta})$.

The next proposition presents a solution for the tracking control problem. Again, the solution is based on the interconnection of a dynamical controller system that drives the closed-loop system to the desired state and leaves an external output $u^\star$ free to regulate the power distribution.

Proposition 2. Consider the MG system represented by (7) interconnected with the controller system Σ_C

$$\Sigma_C := \begin{cases} \dot{z} = u_c \\ y_c = \nabla H_c(z) \end{cases} \quad (11)$$

with state $z \in \mathbb{R}^n$, $u_c \in \mathbb{R}^n$, $H_c : \mathbb{R}^n \to \mathbb{R}$ given by

$$H_c(z) = \frac{1}{2} z^\top K_i z, \quad (12)$$

and $K_i = K_i^\top > 0$ a positive gain, via the power preserving interconnection:

$$\begin{bmatrix} u \\ u_c \end{bmatrix} = \begin{bmatrix} -K_p & -\mathbf{I} \\ \mathbf{I} & 0 \end{bmatrix} \begin{bmatrix} \tilde{y}_e \\ y_c \end{bmatrix} + \begin{bmatrix} u^\star \\ 0 \end{bmatrix} \quad (13)$$

where $K_p = K_p^\top > 0 \in \mathbb{R}^{n\times n}$ is a controller gain. Assume that:

A1. The VSI's parameters are positive and known.
A2. The demanded current i_o is a known bounded and continuous function.
A3. The references $x^\star$ are known bounded functions with bounded first derivative.
A4. Each reference $v_{v_k}^\star$, with $k = 1, \ldots, n$ is a bounded function.

Then, the closed-loop system fulfills the control objective (9).

Proof. We take the time derivative of the radially unbounded function

$$H_T(\tilde{x}_e, z) = \tilde{H}_e(\tilde{x}_e) + H_c(z) \quad (14)$$

along (10) in closed-loop with (11)-(13) which gives

$$\begin{aligned} \dot{H}_T &= \nabla^\top \tilde{H}_e \dot{\tilde{x}}_e + \nabla^\top H_c \dot{z} \\ &= \nabla^\top \tilde{H}_e \left(-R_e \nabla \tilde{H}_e + \begin{bmatrix} G_m \\ 0 \end{bmatrix} (-K_p \tilde{y}_e - y_c) \right) + \nabla H_c^\top \tilde{y}_e \\ &= -\nabla^\top \tilde{H}_e R_e \nabla \tilde{H}_e - \tilde{y}_e K_p \tilde{y}_e \leq 0 \end{aligned}$$

showing that the closed-loop system is stable in the sense of Lyapunov. Moreover, since the maximal invariant set for which $H_T \equiv 0$ is $\tilde{x} = 0$ then, using standard arguments, the asymptotic stability of $\tilde{x} = (\tilde{i}, \tilde{v}) = (0, 0)$ can be concluded if $x_e^\star$ is bounded. □

Remark 3. The $x_e^\star$ value involves the desired state $x^\star$ and the virtual voltage vector $v_v^\star = \text{col}\left(v_{v_k}^\star\right)$. The $v_v^\star$ value is determined by the gain selection related to Proposition 1, so in terms of the proof, we do not need to know it *a priori*, but it is necessary to assume that it is bounded.

4. DROOP CONTROLLER

Once the state x is guaranteed to reach its desired $x^\star$, the problem is to define a correspondence between those desired trajectories $x^\star$ and the power distribution. To solve this problem, we use the external input $u^\star$ to add a droop-type controller. We present the basis of this controller in the following.

In steady-state, a VSI can be represented by an ideal voltage source in series with its output impedance. Fig. 2 illustrates one VSI with output voltage amplitude E and power angle δ, delivering power to an AC bus $V\angle 0°$ (or another voltage source) through an impedance $Z_o\angle\theta$.

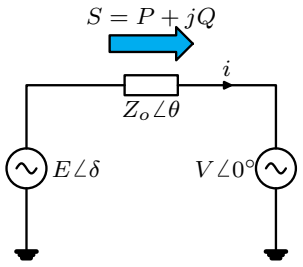

Fig. 2. Equivalent circuit of a VSI connected to an AC bus

The complex power drawn to the bus is written as

$$S = P + jQ \quad (15)$$

where P and Q are the active and reactive power, respectively, which can be expressed, following Zhong and Hornik [2012], as:

$$\begin{bmatrix} P \\ Q \end{bmatrix} = \begin{bmatrix} \sin\theta & \cos\theta \\ -\cos\theta & \sin\theta \end{bmatrix} \begin{bmatrix} \frac{EV_0}{Z_0}\sin\delta \\ \frac{EV_0}{Z_0}\cos\delta - \frac{V_0^2}{Z_0} \end{bmatrix} \tag{16}$$

where the power angle δ is the phase difference between the supply and the terminal.

The so-called conventional droop control law is based on some proportionality, for a small power angle δ, between the magnitude and phase variables and the active and reactive powers. The output impedance determines this proportionality. When the output impedance is inductive $\theta = 90°$, and if $\sin\delta \approx \delta$ and $\cos\delta \approx 1$, it can be obtained that the active power P is strongly dependent on the angle δ. At the same time, the amplitude difference $E - V_0$ mainly influences the reactive power Q, so that

$$P \sim \delta \quad \text{and} \quad Q \sim E. \tag{17}$$

As mentioned in Guerrero et al. [2005], this effect is well known in large scale systems in which the generators drop their frequency as the output power increases. Hence trying to follow this behavior, the $Q-E$ and $P-\omega$ droop is used to design the control strategy for the $k-th$ VSI. This conventional droop controller takes the form:

$$E_k = E^\star - n_k Q_k, \tag{18a}$$
$$\omega_k = \omega^\star - m_k P_k \tag{18b}$$

for $k = 1, \ldots, n$, where $\omega^\star$ and $E^\star$ are the nominal output voltage frequency and amplitude, while m_k and n_k are the droop coefficients.

Similar to the previous analysis, when the output impedance is resistive $\theta = 0°$, for small δ, $P \sim E$ and $Q \sim -\delta$, so that the $Q-\omega$ and $P-E$ droop is used to generate the control strategy, but different to (18), the $Q-\omega$ loop is a negative loop so that the sign before $m_k Q_k$ is positive. Finally, if the output impedance is capacitive, then $\theta = -90°$ and for a small δ it turns that $P \sim -\delta$ and $Q \sim -E$. In this case, to ensure that the $Q-E$ loop and the $P-\omega$ loop are negative feedback, the signs before $n_k Q_k$ and $m_k P_k$ are all positive.

In this paper, we take the improved droop control strategy of Zhong and Hornik [2012]. The controller, implements the voltage E_k in (18) via integrating $\Delta E_k = E_k - E^\star = -n_k P_k$ as

$$E_k = \int_o^t \Delta E_k dt, \tag{19}$$

and adds to ΔE_k the load voltage drop $E_k^\star - V_k$, with V_k the RMS value of the filter's output voltage v_k (see Fig.3). So that, in the case of the inductive output impedance, the robust droop controller for the $k-th$ VSI is of the form:

$$\dot{E}_k = -n_k Q_k + k_{e_k}(E^\star - V_k), \tag{20a}$$
$$\omega_k = \omega^\star - m_k P_k \tag{20b}$$

with $k_{e_k} \in \mathbb{R}$ a positive gain. A similar procedure can define the robust-droop controllers when the output impedance is resistive or capacitive.

Finally, we assign to each reference $u_k^\star$ in (13) a sinusoidal where its magnitude and phase are specified by the robust droop controller, selected according to the designed output impedance, so that:

$$u_k^\star = \sqrt{2} E_k \sin(\omega_k t + \delta_k), \tag{21}$$

where ω_k is integrated to form the phase of the control reference $u_k^\star$.

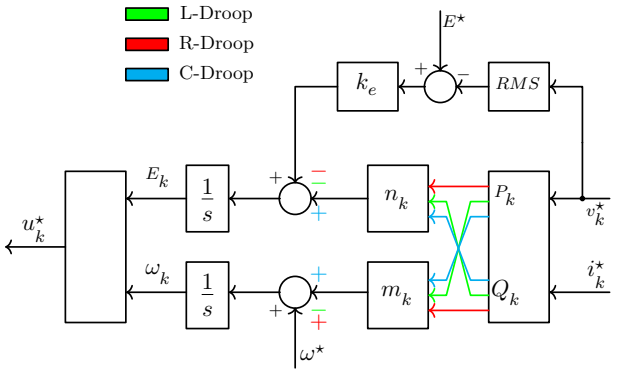

Fig. 3. Robust droop controller for L-inverters, R-inverters and C-inverters.

5. NUMERICAL EVALUATION

To validate the result, we use four inverters parallel connected with both a non-linear and a linear load as presented in Fig.4. The inverters are controlled by (11) with the power preserving interconnection (13) and the output impedance control (4). In order to achieve load distribution, the desired trajectories are obtained by means of a droop controller, depending on the inverter's output impedance. The generation units have the same

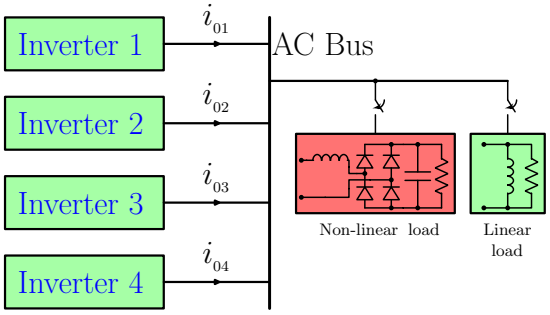

Fig. 4. Four inverters in parallel with linear load and non-linear load.

parameters but we assume that the units have different apparent power capacity. In this sense, each inverter is powered by $v_{dk} = 500\ V$ DC voltage source, and the power ratings are $S_1 = 10\ kVA$, $S_2 = 20\ kVA$, $S_3 = 30\ kVA$, $S_4 = 40\ kVA$. The filters' inductances and capacitances are $L_k = 2.35\ mF$ and $C_k = 28\ \mu F$ with $r_{L_k} = 0.9\ \Omega$ and $r_{C_k} = 100\ M\Omega$, respectively. The

droop coefficients are $n_k = \frac{k_e V_{ref}}{4S_k}$ and $m_k = \frac{\omega_{ref}}{10S_k}$, while $V_{ref} = 120\ V_{RMS}$ and $\omega_{ref} = 2\pi f_{ref}$ with $f_{ref} = 50\ Hz$ and $k_e = 50$. The controllers' gains are $K_{p_k} = 100$ and $K_{i_k} = 200$. The impedance control parameters are shown in Table 1

Table 1. Virtual elements

Inverter	C_v	r_{Cv}	r_v	Z_o
L-Inverter	1 $[MF]$	1 $[M\Omega]$	0 $[\Omega]$	$0.1 + 0.7383i$ $[\Omega]$
R-Inverter	1 $[MF]$	1 $[M\Omega]$	15 $[\Omega]$	$15.1 + 0.7383i$ $[\Omega]$
C-Inverter	1.5 $[mF]$	100 $[\Omega]$	0 $[\Omega]$	$0.145 - 1.3828i$ $[\Omega]$

We use a rectifier bridge with parameters $L = 1mH$, $C = 470\mu F$ and $r = 10\omega$ as non-linear load; see Figure 4.

5.1 Simulation results

The numerical evaluation was performed in the Simulink environment of MATLAB^{TM}, considering a fixed-step solver. The validation of the proposed controller consists of connecting a linear and a non-linear load. The inverters have to regulate the voltage and distribute the power according to their capacities. The output impedance of the inverters is modified so that there are L-inverters, R-inverters and C-inverters. The numerical validation is divided into three time intervals, at time $0 < t < 0.5$ there is no load connected to the inverters. At time $0.5 < t < 2$ a linear load is connected, at time $2 < t < 3.5$ a non-linear load is connected, in time $3.5 < t < 5$ the linear load is disconnected, therefore the connected load is non-linear. Finally, at time $5 < t < 7$ the non-linear load is disconnected of the system, and the inverters are left working at a non load condition.

In Figure 5 the behavior of the L-inverters is observed, with the load profile described above. Figure 5(a) shows the active power of the load P_0 and the power of the inverters P_k, with $k = 1, 2, 3, 4$. Note that there is a distribution of active power among the inverters, which is best observed in the time interval $2 < t < 3.5$, since $P_2 = 2P_1$, $P_3 = 3P_1$ and $P_4 = 4P_1$. In Figure 5(b) the reactive power of the load and the inverters is observed. In this case, it is observed that all the inverters provide reactive power to satisfy the load demand; however, the load distribution is not precise. Figure 5(c) shows the RMS reference voltage and the load's voltage. The voltage does not exceed 10% of the reference voltage at any time. The harmonic voltage distortion with nonlinear load is $THD = 6.71\%$.

Figure 6 shows the active and reactive power, and the voltage of the R-inverters. In this case, a precise active power distribution is also fulfilled; however, the convergence time increases, compared to L-inverters. For the reactive power, it is observed that the distribution between the sources is precise. In this case, the voltage peaks due to load changes exceed 50% of the nominal value, as seen in Figure 6(c). The harmonic voltage distortion with the nonlinear load is $THD = 9.51\%$.

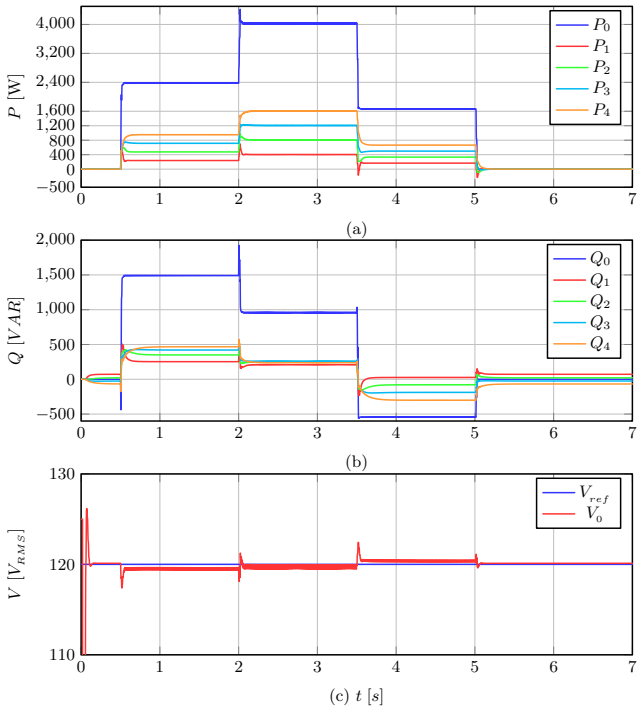

Fig. 5. L-Inverter with L-Droop; a)Active power b)reactive power c)load voltage

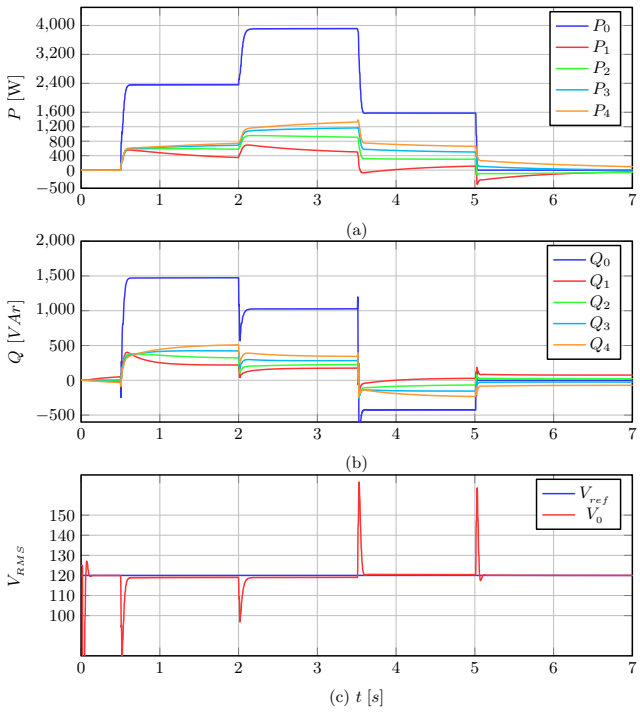

Fig. 6. R-Inverter with R-Droop;a)Active power b)reactive power c)load voltage

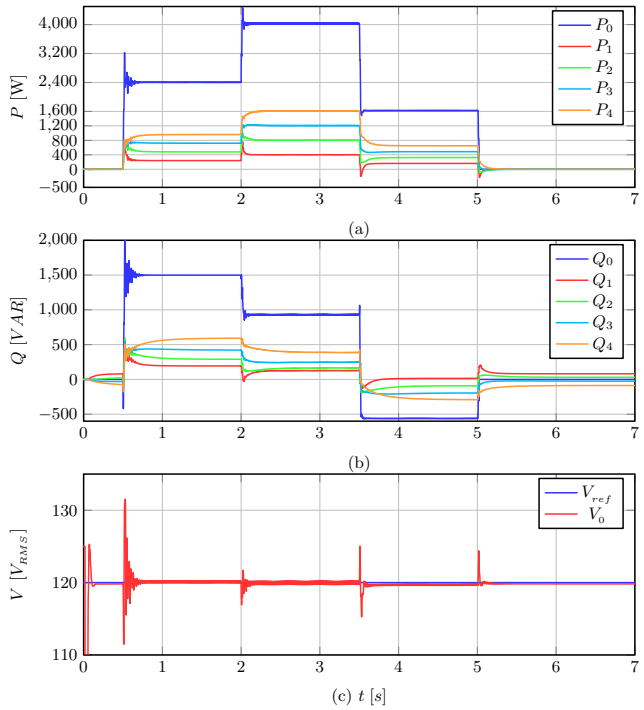

Fig. 7. C-Inverter with C-Droop; a)Active power b)reactive power c)load voltage

Concerning to the C-inverters, a precise active and reactive power distribution is observed. The voltage peaks due to load variations do not exceed 10% of the nominal voltage, as shown in Figure 7(a). The harmonic voltage distortion with nonlinear load is $THD = 6.54\%$.

As one can see, regardless of the output impedance, the three controllers generate a voltage drop that limits an accurate voltage regulation; this is a consequence of the droop technique; new control loops called secondary are usually implemented for its compensation; see for example Guerrero et al. [2011].

6. CONCLUSION

A robust droop controller analysis methodology is proposed for L-inverters, R-inverters and C-inverters, from an interconnected Hamiltonian systems perspective. Unlike the reported in the literature, in this paper, the droop control is used to generate the desired trajectories of the physical system and if these trajectories are bounded, then asymptotic and global stability of the equilibrium point $x - x^\star = 0$ is guaranteed.

REFERENCES

Avila-Becerril, S., Montoya, O.D., Espinosa-Pérez, G., and Garcés, A. (2018). Control of a detailed model of microgrids from a hamiltonian approach. *IFAC-PapersOnLine*, 51(3), 187–192.

Bendib, A., Kherbachi, A., Kara, K., and Chouder, A. (2017). Droop controller based primary control scheme for parallel-connected single-phase inverters in islanded ac microgrid. In *2017 5th International Conference on Electrical Engineering-Boumerdes (ICEE-B)*, 1–6. IEEE.

Cisneros, R., Pirro, M., Bergna, G., Ortega, R., Ippoliti, G., and Molinas, M. (2015). Global tracking passivity-based pi control of bilinear systems: Application to the interleaved boost and modular multilevel converters. *Control Engineering Practice*, 43, 109–119.

De Persis, C. and Monshizadeh, N. (2017). Bregman storage functions for microgrid control. *IEEE Transactions on Automatic Control*.

Guerrero, J.M., De Vicuna, L.G., Matas, J., Castilla, M., and Miret, J. (2005). Output impedance design of parallel-connected ups inverters with wireless load-sharing control. *IEEE Transactions on industrial electronics*, 52(4), 1126–1135.

Guerrero, J.M., Vasquez, J.C., Matas, J., De Vicuña, L.G., and Castilla, M. (2011). Hierarchical control of droop-controlled ac and dc microgrids—a general approach toward standardization. *IEEE Transactions on industrial electronics*, 58(1), 158–172.

Han, H., Hou, X., Yang, J., Wu, J., Su, M., and Guerrero, J.M. (2016). Review of power sharing control strategies for islanding operation of ac microgrids. *IEEE Transactions on Smart Grid*, 7(1), 200–215.

Mortezapour, V. and Lesani, H. (2017). Hybrid ac/dc microgrids: A generalized approach for autonomous droop-based primary control in islanded operations. *International Journal of Electrical Power & Energy Systems*, 93, 109–118.

Ortega, R., van der Schaft, A., Castanos, F., and Astolfi, A. (2008). Control by interconnection and standard passivity-based control of port-hamiltonian systems. *Automatic Control, IEEE Transactions on*, 53(11), 2527–2542.

Rojas, A. and Rousan, T. (2017). Microgrid control strategy: Derived from stakeholder requirements analysis. *IEEE Power and Energy Magazine*, 15(4), 72–79.

Rokrok, E., Shafie-Khah, M., and Catalão, J.P. (2018). Review of primary voltage and frequency control methods for inverter-based islanded microgrids with distributed generation. *Renewable and Sustainable Energy Reviews*, 82, 3225–3235.

Schiffer, J., Zonetti, D., Ortega, R., Stanković, A.M., Sezi, T., and Raisch, J. (2016). A survey on modeling of microgrids—from fundamental physics to phasors and voltage sources. *Automatica*, 74, 135–150.

Zhong, Q.C. (2011). Robust droop controller for accurate proportional load sharing among inverters operated in parallel. *IEEE Transactions on industrial Electronics*, 60(4), 1281–1290.

Zhong, Q.C. and Hornik, T. (2012). *Control of power inverters in renewable energy and smart grid integration*, volume 97. John Wiley & Sons.

